Differences Between Passive-Phase Conjugation and Decision-Feedback Equalizer for Underwater Acoustic Communications

T. C. Yang

***Abstract*—Passive-phase conjugation (PPC) uses passive time reversal to remove intersymbol interferences (ISIs) for acoustic communications in a multipath environment. It is based on the theory of signal propagation in a waveguide, which says that the Green's function (or the impulse-response function) convolved with its time-reversed conjugate, summed over a (large-aperture) vertical array of receivers (denoted as the Q function) is approximately a delta function in space and time. A decision feedback equalizer (DFE) uses a nonlinear filter to remove ISI based on the minimum mean-square errors (mmse) between the estimated symbols and the true (or decision) symbols. These two approaches are motivated by different principles. In this paper, we analyze both using a common framework. We note the commonality and differences, and pros and cons, between the two methods and compare their performance in realistic ocean environments, using simulated and at-sea data. The performance measures are mean-square error (mse), output signal-to-noise ratio (SNR), and bit-error rate (BER) as a function of the number of receivers. For a small number of receivers, the DFE outperforms PPC in all measures. The reason for poor PPC performance is that, for a small number of receivers, the Q function has nonnegligible sidelobes, resulting in nonzero ISI. As the number of receivers increases, the BER for both processors approaches zero, but at a different rate. The modeled performance differences (in mse and SNR) between PPC and DFE are in general agreement with the measured values from at-sea data, providing a basis for performance prediction.**

***Index Terms*—Decision feedback equalizer (DFE), passive-phase conjugation (PPC), underwater acoustic communications.**

I. Introduction

SEVERAL methods have been proposed for phase-coherent underwater acoustic communications using phase-shift keying (PSK) modulations. Among them, a channel equalizer, particularly a decision-feedback equalizer (DFE), jointly with a phase-locked loop (PLL) has shown promising results [1]. A recently proposed method uses a time-reversal mirror [2], [3] or, equivalently, a passive-phase conjugation (PPC) approach [4], [5]; the former requires two-way transmission and the latter does not. The time-reversal mirror [6] and PPC [7] methods are based on the back-propagation properties of an acoustic waveguide that focuses/compresses the received acoustic signal back to the original signal, thereby reducing the intersymbol interferences (ISI). Bit errors reduce to zero or a minimal amount when a sufficient number of receivers are used [8]. The channel equalizer is based on adaptive filtering of a linear system that minimizes the mean-square errors (mse) between the estimated and true symbols [9]–[11]. Note that the above two methods were (independently) developed by engineers and physicists; the former uses signal processing and the latter uses the physics of propagation. Thus, questions have been raised as to the commonality and differences between the two methods, as well as the advantages and drawbacks of each method. A prevailing assumption among the signal processors is that the channel effect can be removed if the channel can be estimated and tracked. So, the question from the point of signal processing has been "Does PPC provide a better channel estimation?" A common assumption among physicists is that the channel-impulse response plays a critical role in the performance of an underwater acoustic modem; hence, measurements and knowledge of how the channel-impulse response evolves with the oceanographic environment is critical to prediction of the performance. This paper addresses the question of the differences between the methods, as well as their pros and cons. The results will shed light on the related questions.

A word on the basic problem is in order here. The reasons for using the phase-coherent communication approach is that it allows symbols to be transmitted continuously within a packet, providing a higher data rate for a given bandwidth. The phase-incoherent approach, using, e.g., frequency-shift keying signals, must wait for the multipaths to die down before another bunch of symbols can be transmitted and, thus, is less bandwidth efficient. For radio communications where the bandwidth is large and multipath arrivals are limited, the difference in the data rates is not a significant factor. In underwater acoustic communications, the bandwidth is limited and the multipaths can last tens of milliseconds to seconds, creating ISIs covering tens to hundreds of symbols. As a result, the data rates between the two approaches can differ by an order of magnitude or more. The result favors the phase-coherent approach. However, the phase-coherent approach is more difficult. To make it work, one must remove the ISI. Hence, removing ISI will be the key measure of the algorithm performance. The ultimate measurement of ISI lies in the resulting BER.

For underwater acoustic communications, the time variability of the channel is another concern. The interest of this paper is the performance comparison between the PPC and DFE. Since both time reversal and PPC assume time invariance, we shall confine ourselves to a time-invariant channel in this paper.

We will illustrate the differences between primarily two methods (PPC and DFE) with a theoretical analysis, with

Manuscript received July 15, 2003; revised February 18, 2004. The work was supported by the Office of Naval Research.

The author is with the Naval Research Laboratory, Washington, DC 20375 USA (e-mail: yang@wave.nrl.navy.mil).

Digital Object Identifier 10.1109/JOE.2004.827122

U.S. Government work not protected by U.S. copyright.

analysis that uses simulated data in a real ocean environment and, lastly, with data collected at sea. Three measures of performance are used: BER, average mse, and output signal-to-noise ratio (SNR) for data of a fixed-input SNR. The simulated data and ocean data analyzed here are the same as in a previous paper [8], where the BER was evaluated as a function of the number of receivers using the PPC approach. In this paper we add the analysis of DFE and also extend the analysis to include mse and output SNR. We also include the results of a linear equalizer for comparison purpose. We note that the performance analysis for PPC can be equally applied to the time-reversal case.

This paper is organized as follows. Section II briefly reviews the PPC method. Section III briefly reviews the linear equalizer (LE) and nonlinear DFE using the minimum mse (mmse) and the iterative recursive least-square (RLS) algorithms. The fundamental differences between PPC, LE, and DFE should become clear from the discussions. Section IV estimates the BER, mse, and output SNR as a function of the number of sensors using simulated data and compares the results between the various methods. Section V compares the results between PPC and DFE with at-sea data. Section VI is a summary.

The analysis of this paper follows the following logical steps. We first show the theoretical differences between the various methods for a single channel without the presence of noise. Since noise is invariably present, we next discuss the optimal solution, the mmse approach. A closed-form solution for mmse is given and is used numerically in a simulation. In practice, we find that the mmse solution is not very useful when many multipaths are present (requiring inversion of a large matrix) and/or when the channel is time varying. Hence, we next turn our attention to the RLS method. The validity of the RLS algorithm is illustrated for a time-invariant channel with a small number of multipath arrivals—the RLS method yields practically the same solution as the closed-form mmse solution. Armed with this "certification," the RLS algorithm is applied to simulated and real-world data. The RLS results are obtained for LE and DFE and are then compared with the results derived from PPC. We note that, based on the theoretical analysis and the mmse solutions for a single channel, the DFE performance is clearly superior to that of PPC. This is also true for multiple receivers in a realistic ocean acoustic environment. With increasing number of receivers, all methods yield BER approaching or equaling zero. We note that DFE has problems of its own, such as sensitivity to the choice of parameters. The DFE is well-known for error propagation, which sometimes causes the RLS algorithm to diverge. This problem restricts the use of unsupervised adaptation to real data. It was also noted that the DFE usually works only with data of high temporal coherence (>0.5) [12].

Since the mmse and RLS algorithms have been discussed elsewhere [9]–[11], only a brief summary will be given in this paper. This summary is given not just for completeness; it spells out the formulas actually used in the numerical calculations.

II. PPC

PPC and time-reversal communications share the same principle and have been addressed elsewhere [2]–[5], [8]. PPC uses a large vertical array of receivers to suppress the ISI. This section establishes the notation and summarizes its basic features, for comparison with the channel equalizer discussed below.

The communication signal consists of a sequence of symbols denoted as I_n. Each symbol has a duration of T. The transmitted signal can be expressed as

$$s(t) = \sum_n e^{i2\pi f_C t} g(t - nT) I_n \tag{1}$$

where f_c is the carrier frequency and g denotes the pulse shape for each symbol

$$\begin{aligned} g(\tau) &= 1, \quad \text{for } 0 < \tau < T \\ g(\tau) &= 0, \quad \text{elsewhere.} \end{aligned}$$

The received signal can be expressed as

$$r_j(t) = h_j(t) \otimes s(t) + z_j(t) \tag{2}$$

where $z_j(t)$ represents band-limited noise and h_j represents a band-limited channel-impulse response for the jth receiver, i.e., the convolution of the transmitter filter and/or receiver filter with the impulse-response function.

Passive phase conjugation uses a probe signal received in advance of the data packet to correlate with the received data. The probe signal is used to estimate the band-limited channel-impulse response h_{j}. PPC of the signal in (2) implies

$$\begin{aligned} \hat{r}(t) &= \sum_j h_j(-t) \otimes r_j(t) \\ &= \sum_j h_j(-t) \otimes (h_j(t) \otimes s(t) + z_j(t)) \\ &\equiv Q(t) \otimes s(t) + \varsigma(t) \end{aligned} \tag{3}$$

where $\varsigma(t) = \sum_j h_j(-t) \otimes z_j(t)$ is a filtered noise and Q is the autocorrelation of the impulse-response functions summed over the channels [8].

Taking the Fourier transform of the Q function, one obtains

$$\begin{aligned} Q(\omega) &= \sum_j H_j^*(\omega) H_j(\omega) \\ &= \frac{2\pi}{r_j} \sum_{m,n} \exp\left(j\left(k_n^* - k_m\right) r_j\right) \psi_n(z_S) \psi_m(z_S) \\ &\quad \times \sum_j \psi_n(z_j) \psi_m(z_j) / \sqrt{k_n k_m} \end{aligned} \tag{4}$$

where the superscript * denotes complex conjugate and $H_j(\omega)$ is the Fourier transform of the impulse response and is expressed in terms of normal modes as

$$H_j(\omega) = \sum_m \sqrt{2\pi} \exp(-j k_m r_j) \psi_m(z_j) \psi_m(z_S) / \sqrt{k_m r_j} \tag{5}$$

where m is the mode number, k_m is the mode wavenumber, and ψ is the mode depth function evaluated at frequency ω and receiver depth z_j. Since $r_j = r$ for a vertical array, assuming mode orthogonality

$$\sum_j \psi_n(z_j) \psi_m(z_j) = \delta_{m,n} \tag{6}$$

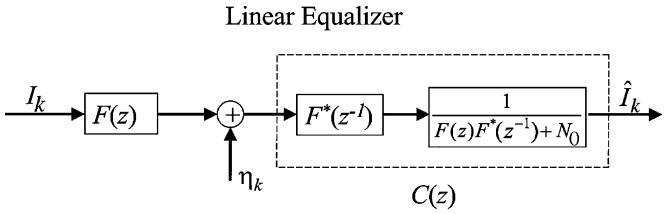

Fig. 1. Block diagram for the LE using the mmse solution. $F(z)$ is the z transform of the channel impulse-response function, where $z = \exp(j\omega t)$. The equalizer $C(z)$ reduces to $1/F(z)$, the inverse of the impulse-response function, when there is no noise. See [9] for details.

one finds

$$Q(\omega) = \frac{2\pi}{r}\sum_m \psi_m(z_S)\psi_m(z)\exp(-2\alpha_m r)/k_m \equiv Q_0 \quad (7)$$

where α_m is the mode-attenuation coefficients. We then have

$$Q(t) = \int_{f_c-\frac{B}{2}}^{f_c+\frac{B}{2}} Q_0\exp(j\omega t)d\omega = 2\overline{Q}_0\exp(j2\pi f_c t)\frac{\sin(\pi Bt)}{t} \quad (8)$$

where $\overline{Q}_0$ is the mean value of Q_0. We note that $Q(t)$ behaves like a $sinc$ function with a width equal to the bandwidth B and has small side lobes, which is a characteristic feature of a waveguide. This feature is the key for acoustic communications using PPC. Numerical simulations in [8] showed that the sidelobe levels decrease with an increasing number of receivers, yielding a sidelobe structure similar to the $sinc$ function. The same cannot be said for free space, where the sidelobe levels will not always decrease when more receivers are used.

III. Channel Equalizer

Channel equalization is commonly done in the baseband. Equation (2) can be expressed in the baseband as

$$r(t) = \sum_n I_n h(t-nT) + z(t) \quad (9)$$

where $r(t)$ now denotes the baseband signal. For a linear system analysis, the noise $z(t)$ is treated as additive white Gaussian noise. To simplify the matter, we confine our discussions mostly to a single channel. Unless specifically mentioned, we will drop the channel index. The result can be generalized to multichannels. Following Proakis [9], one can create an equivalent discrete channel having a minimum phase

$$v(t) = \sum_n I_n f(t-nT) + z(t). \quad (10)$$

For simplicity, we will assume a minimum phase channel, which physically means that the amplitude of the impulse-response function decreases monotonically with delay time. In that case, $f = h$ and $v = r$. We note that, in the real world, the channel is not always minimum phase; the nonminimum phase case will be dealt with elsewhere.

Taking one sample per symbol, one has

$$v_k = \sum_{n=0}^{L} f_n I_{k-n} + \eta_k \quad (11)$$

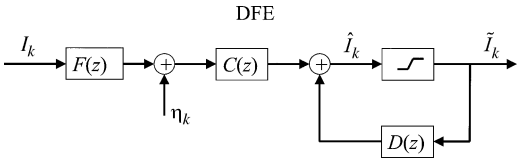

Fig. 2. Block diagram for the DFE.

where k is sample index, $\{f_n\}$ is a discrete representation of the band-limited impulse-response function of length $L+1$, and $\{\eta_k\}$ is a white Gaussian noise sequence.

An LE multiplies (11) by a set of tap coefficients c_j

$$\hat{I}_k = \sum_{j=-\infty}^{\infty} c_j v_{k-j}. \quad (12)$$

If c_j equals the inverse of the impulse-response function, it is called a zero-forcing filter. The inverse of the impulse-response function is an infinite length filter. Errors occur when only a finite length filter is used in practice. Equation (12) is illustrated via a block diagram in Fig. 1.

A nonlinear equalizer has the form

$$\hat{I}_k = \sum_{j=-K_1}^{0} c_j v_{k-j} + \sum_{j=1}^{K_2} d_j \widetilde{I}_{k-j} \quad (13)$$

where c_j and d_j are the tap coefficients for the feed-forward and feedback loops, respectively, and $\widetilde{I}_{k-j}$ denotes a decision symbol, namely the symbol that best matches the estimated symbol I_{k-j}. Hence, it is called a DFE (see the block diagram in Fig. 2).

To motivate the discussions below, let us ignore the noise for a moment. One can solve (11) for the kth symbol I_k in terms of incoming data v_k and previously resolved symbols as

$$I_k = f_0^{-1}v_k - \sum_{n=1}^{L} f_0^{-1} f_n I_{k-n}. \quad (14)$$

Comparing (14) with (13), we see that (14) has the form of a DFE with one feed-forward tap coefficient $c_{-1} = (f_0)^{-1}$ and L feedback tap coefficients, as given above. The decision symbol is the same as the true symbol.

One can also use (14) again for I_{k-1} and obtain

$$I_k = f_0^{-1}v_k - \left(\frac{f_1}{f_0^2}\right)v_{k-1} - \sum_{n=2}^{L}\left(\frac{f_1 f_{n-1}}{f_0^2} - \frac{f_n}{f_0}\right)I_{k-n} + \left(\frac{f_1 f_L}{f_0^2}\right)I_{K-L-1}. \quad (15)$$

Comparing (15) with (13), we see that (15) is equivalent to a DFE with two feed-forward coefficients and L feedback coefficients. Continuing this process, one can be convinced that, independent of the number of feed-forward coefficients used, L feedback coefficients are always required. However, the values of the feedback coefficients change with the number of feed-forward coefficients used. It will be illustrated below that the mmse solution corresponds to the case of a minimum number of feed-forward coefficients.

We note that a linear system solves for the tap coefficients using a certain criterion (such as minimum mse, as discussed below) from a given data set (the training symbols). As such, the results vary depending on the number of tap coefficients assumed. Equation (14) (or the equation with more feed-forward coefficients) serves as the physical foundation of a DFE. It says that the feedback loop is not just a numerical necessity for minimizing bit errors; it is required by the channel physics. Second, it should have a length equal to the multipath delay minus one. Third, its values are uniquely determined from the channel-impulse response. From (14) and (15), we note that the values of the feed-forward and feedback tap coefficients are interrelated.

Using (11), we can evaluate the PPC method in the same context. Convolving (11) with the time-reversed impulse-response function (the probe signal), after some mathematical manipulations one obtains

$$\sum_{l=0}^{L} f_l^* v_{k-l} = x_0 I_k + \sum_{n=1}^{L} x_n I_{k-n} + \sum_{n=1}^{L} x_n^* I_{k+n} \tag{16}$$

where

$$x_n = \sum_{l=1}^{L-n} f_l^* f_{l+n} \tag{17}$$

is the discrete representation of the autocorrelation of the channel impulse-response function, i.e., the Q function for a single channel.

Summing (16) over the different receivers (with subscript j), we obtain the multichannel expression, which can be rewritten as

$$I_k = x_0^{-1} \left\{ \sum_j \sum_{l=0}^{L} f_{j,l}^* v_{j,k-l} - \sum_{n=1}^{L} x_n I_{k-n} - \sum_{n=1}^{L} x_n^* I_{k+n} \right\} \tag{18}$$

where the first term on the right-hand side of (18) is the output of the PPC process and x_n now denotes the discrete representation of the Q function for multiple channels. As discussed in the previous section, PPC for multiple channels uses the properties of the channel waveguide to suppress the side lobes of the Q function. In other words, by summing over receivers on a large aperture array, one finds $x_n \approx 0$ for $\mathrm{n} \neq 0$. Note that the second and third terms in (18) are the cause for bit errors. Equation (18) says that bit errors are negligibly small for PPC when a large-aperture vertical array of receiver is used.

Conversely, when a small number of receivers are used, the Q function has nonnegligible side lobes ($x_n \neq 0$, for $\mathrm{n} \neq 0$), and PPC will generally have significant bit errors. Equation (18) says that, in this case, PPC needs a "feedback" correction, as shown by the second and third terms, in order to get rid of the bit errors.

The block diagram for PPC is illustrated in Fig. 3 for a signal channel (without the feedback loop). One sees that it is a special form of a LE (a simplified version of Fig. 1) where the tap coefficients are the time-reversed impulse-response function. Note that the cross-correlation of the data with the probe signal (the impulse-response function) is a matched-filter process, a common procedure in digital communications [9]. The probe signal is a linear transversal filter of a finite length. The deficiency of a linear transversal filter of a finite length in removing ISI is well known (see the discussions in [9]).

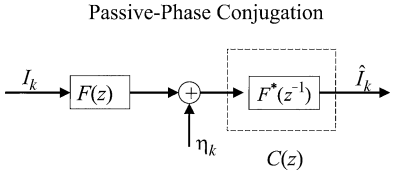

Fig. 3. Block diagram for the PPC equalizer.

A. The mmse Solution

The mmse algorithm can be found in many textbooks. The results are summarized here and will be used in actual computations. A derivation can be found in [9], for example.

In the real world, the noise is always present. The mmse solution is obtained by minimizing the mse between the estimated and true symbols, $\langle |I_k - \hat{I}_k|^2 \rangle$ in the presence of noise, where $\langle\rangle$ denotes expected value. Expressing (12) in a vector form, $\hat{I}_k = \sum_j c_j v_{k-j} \equiv \mathbf{v}^T \mathbf{c}$, where $\mathbf{c}$ and $\mathbf{v}$ are column vectors and the superscript T denotes transpose, the mmse solution is given by solving

$$\mathbf{\Gamma c} = \boldsymbol{\xi} \tag{19}$$

for c, where

$$\begin{aligned} \Gamma &= \langle \mathbf{v}^* \mathbf{v}^T \rangle \\ \boldsymbol{\xi} &= \langle I_k \mathbf{v}^* \rangle. \end{aligned} \tag{20}$$

[Equation (19) can also be obtained by multiplying (12) by $\mathbf{v}^*$.] For a time-invariant channel, one finds [9]

$$\Gamma_{ij} = \begin{cases} x_{i-j} + N_0 \delta_{ij} & |i-j| \leq L \\ 0 & \text{otherwise} \end{cases} \tag{21}$$

where N_0 is the variance of the noise and $\boldsymbol{\xi}^* = [f_L, f_{L-1}, \ldots, f_1, f_0]^T$ with the rest of the elements zero.

Equation (13) can also be written in a matrix form. After some steps, the mmse solution for the nonlinear equalizer (13) is given by

$$\mathbf{d} = -\mathbf{B}^\dagger \mathbf{c} \tag{22}$$

where the superscript † denotes Hermitian conjugate and

$$\mathbf{c} = \left(\mathbf{\Gamma}_F - \mathbf{B}\mathbf{B}^\dagger\right)^{-1} \boldsymbol{\xi}_F \tag{23}$$

where $\boldsymbol{c}$ and $\boldsymbol{d}$ are column vectors of the feed-forward and feedback coefficients of dimension K_1+1 and K_2, respectively, and $\mathbf{B}$ is a matrix of dimension $(K_1+1) \times K_2$, whose element is given by

$$\mathbf{B}_{ij} = f_{K_1+j-i+1} \tag{24}$$

and $\mathbf{\Gamma}_F$ is a matrix of dimension $(K_1+1) \times (K_1+1)$ with elements given by the top line of (21) and $\boldsymbol{\xi}_F = [f_{K_1}, f_{K_1-1}, \ldots, f_1, f_0]^T$. One can verify that the matrix solution, using (22) and (23), is the same as the explicit solution given in [9].

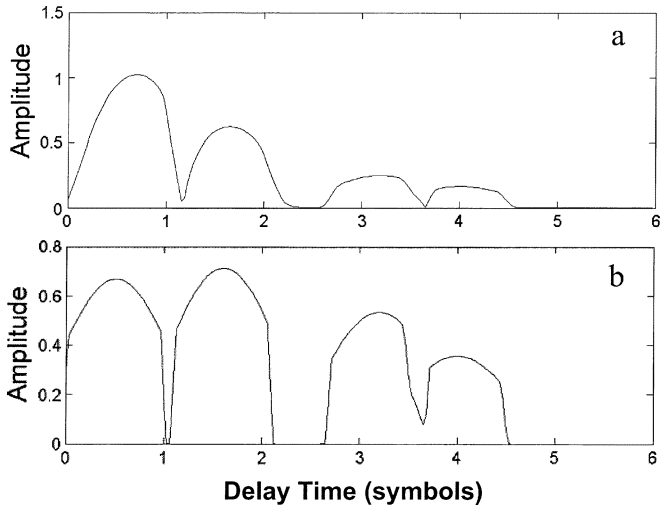

Fig. 4. Band-limited impulse-response functions [impulse responses (a) A and (b) B, respectively) simulating direct, surface, bottom, and surface–bottom bounce arrivals.

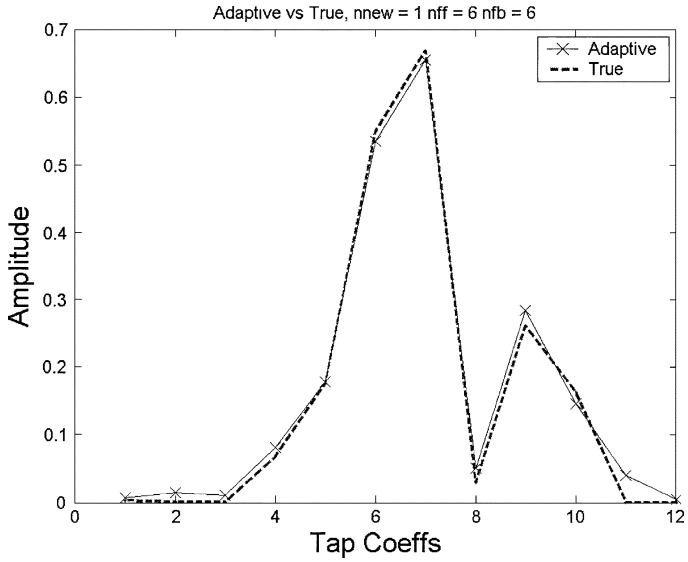

Fig. 5. Comparison of tap coefficients determined by the RLS algorithm (solid line with "x") and mmse formula (dashed line) for impulse response B of Fig. 4. Feed-forward and feedback are designated by taps 1–6 and 7–12, respectively.

We note that, in (22) and (23), one can choose any number of feed-forward and feedback coefficients, K_1 and K_2. However, based on the discussions above [see (14) and (15)], K_2 should be equal or greater than L. The goal is to choose K_1 and K_2 to achieve minimum mse.

As shown in [9], the minimum mse ($J_{\min}$) for an LE of finite length is always larger than that of an infinite LE. The latter can be expressed as [9]

$$J_{\min}^{\mathrm{LE}} = 1 - \frac{T}{2\pi}\int_{-\frac{\pi}{T}}^{\frac{\pi}{T}} \frac{X(e^{j\omega t})}{X(e^{j\omega t}) + N_0} d\omega \tag{25}$$

where X is the Fourier transform of the sequence x_k of (17). For the nonlinear DFE equalizer, $J_{\min}$ is given by [9]

$$J_{\min}^{\mathrm{DFE}} = \exp\left\{\frac{T}{2\pi}\int_{-\frac{\pi}{T}}^{\frac{\pi}{T}} \ln\left[\frac{N_0}{X(e^{j\omega t}) + N_0}\right] d\omega\right\}. \tag{26}$$

The $J_{\min}$ for PPC is given by [13]

$$J_{\min}^{\mathrm{PPC}} = N_0 + \frac{T}{2\pi}\int_{-\frac{\pi}{T}}^{\frac{\pi}{T}} \left[\left|X(e^{j\omega t})\right|^2 - X(e^{j\omega t})\right] d\omega. \tag{27}$$

In (25)–(27), the channel is normalized, i.e., $x_0 = \sum_{l=1}^{L} f_l^* f_l = 1$. Following [9], it can be shown that the following result is always satisfied [13]:

$$J_{\min}^{\mathrm{PPC}} \geq J_{\min}^{\mathrm{LE}} \geq J_{\min}^{\mathrm{DFE}}. \tag{28}$$

which lays the theoretical foundation for the analysis below. Using simulated and real data, we find below that the same conclusion can also be drawn for multiple channels. As such, DFE presents an advantage over PPC in terms of mmse. Note that, for multiple channels, the above inequality is not easily proved theoretically due to interchannel correlations.

B. RLS Solution

For an underwater acoustic channel, multipath arrivals can cover tens to hundreds of symbols. The above matrix solutions [(19), (22), and (23)] require inversion of a large matrix. In practice, an (iterative) RLS solution is commonly used instead. The advantage for using a recursive algorithm is its ability to adapt to a time-varying channel. The RLS solution will be summarized briefly and will be shown to yield the same solution as that obtained by the matrix solution for a time-invariant channel with a small number of tap coefficients. For the simulated and real data, we will use the RLS algorithm because of the above advantage. An alternative to the RLS algorithm is the least-mean square (LMS) algorithm, which is less favored because of its slower convergence rate.

For a time-varying channel, the equalizer coefficient $\mathbf{w}_k$ is a function of the symbol number k. Equation (13) can be written as $\hat{I}_k = \mathbf{V}^T\mathbf{w}_k$, where $\mathbf{w}_k = [\mathbf{c_k}, \mathbf{d_k}]$, and $\mathbf{V} = [\mathbf{v}, \tilde{\mathbf{I}}]$ or, in matrix form, as

$$\mathbf{\Gamma}_k \mathbf{w}_k = \boldsymbol{\xi}_k \tag{29}$$

where one has

$$\begin{aligned}(\Gamma_k)_{ji} &= \langle V_{k-i} V_{k-j}^* \rangle \\ (\boldsymbol{\xi}_k)_j &= \langle I_k V_{k-j}^* \rangle .\end{aligned} \tag{30}$$

The least-square solution to (29) uses a sequential regression algorithm in which the data-covariance matrix in (30) is weighted over previous samples by

$$\hat{\Gamma}_k = \frac{\sum_{l=0}^{k} \lambda^{k-1} \mathbf{V}_l \mathbf{V}_l^{\dagger}}{\sum_{l=0}^{k} \lambda^{k-1}} \tag{31}$$

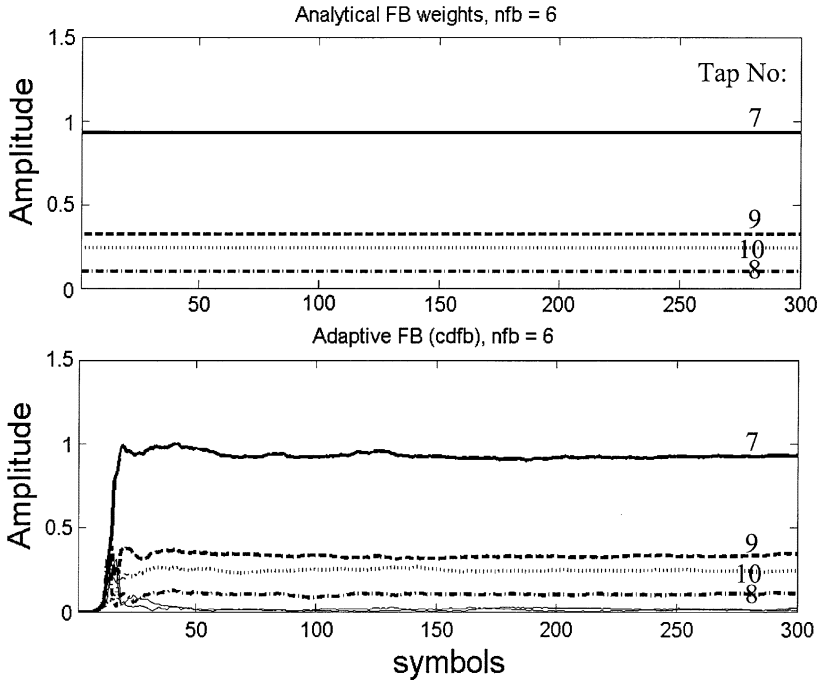

Fig. 6. Evolution of the feedback coefficients as determined by the RLS algorithm (lower figure). The mmse solution for impulse response B of Fig. 4 (upper figure).

where λ is the "forgetting factor" and is usually set close to 1 (e.g., 0.99). Replacing $\mathbf{\Gamma}$ by $\hat{\Gamma}$, (29) can be solved iteratively as [9]–[11]

$$\mathbf{w}_{k+1} = \mathbf{w}_k + \frac{\varepsilon_k^* \mathbf{P}_k \mathbf{V}_k}{\gamma} \tag{32}$$

where $\varepsilon_k = I_k - \hat{I}_k$ is the symbol error, $\gamma = \lambda + \mathbf{V}_k^\dagger \mathbf{P}_k \mathbf{V}_k$, and

$$\mathbf{P}_{k+1} = \frac{\left[\mathbf{P}_k - \frac{(\mathbf{P}_k \mathbf{V}_k)(\mathbf{V}_k^\dagger \mathbf{P}_k)}{\gamma}\right]}{\lambda}. \tag{33}$$

For the above equations, $\mathbf{P}_k$ is the inverse of the data covariance matrix $\mathbf{P}_k^{-1} = (\sum_{l=0}^{k} \lambda^{k-1}) \hat{\Gamma}_k$. In practice, (31) is never actually used. One starts with an initial condition $\mathbf{w}_1 = 0$, $\mathbf{P}_1 = \mathbf{I}$. The tap coefficients $\mathbf{w}$ and matrix $\mathbf{P}$ are updated sequentially given a new data vector $\mathbf{v}_k$ and a new error estimate ε_k. The error ε_k is calculated using the true symbol for the training data and using the decision symbol for the message data.

It can be shown that the above solution is equivalent to the mmse solution by minimizing $\langle \sum_{l=0}^{k} \lambda^{k-1} |I_l - \hat{I}_l|^2 \rangle$. For DFE, the sequential regression algorithm is called the RLS algorithm. The RLS algorithm is more frequently used over the LMS method because it takes a smaller number of inputs to converge to a stable solution.

In the remainder of this section, we will show via two numerical examples that, for a time-invariant channel, the RLS solution indeed yields approximately the same answer as the closed-form mmse solution (22) and (23). We will illustrate the convergence rate of the RLS algorithm and will use the RLS algorithm to show the minimum (and optimal) number of feed-forward coefficients required.

Figs. 4(a) and (b) plot the amplitudes of the impulse responses A and B, respectively, obtained by convolving multipath arrivals with a cosine weighted (low pass) pulse filter, allowing a small (-20 dB) out of band energy. Four multipath arrivals are observed with different delay times and magnitudes. Received data are created by convolving the impulse-response functions with a sequence of quadrature PSK (QPSK) signals. Random Gaussian noise is added to the received data with a SNR of 10 dB. The above RLS algorithm is then used to calculate the tap coefficients for a DFE with six feed-forward and six feedback coefficients and is compared with the mmse solution.

Fig. 5 plots the values of the feed-forward coefficients (1–6) and feedback coefficients (7–12) for impulse response B. The RLS values are denoted by "x." The mmse solution is also plotted as denoted by the dashed curve. We note a close agreement between the RLS solution and mmse solution.

Fig. 6 plots the evolution of the feedback coefficients as a function of the input data sequence in symbols. We see that the RLS takes only 30 symbols to converge to a stable solution. Fig. 7(a) plots the mse between the estimated symbol and true symbols $|\varepsilon_k|^2$. An average mse of -12 dB is obtained. Fig. 7(b) plots the estimated symbol (de) constellations in terms of the real and imaginary parts. The true symbols are located at $[1 + \mathrm{j}, 1 - \mathrm{j}, -1 - \mathrm{j}, -1 + \mathrm{j}]$. In this case, there is no symbol error.

Next, we turn our attention to impulse response A. Impulse responses A and B are quite similar (see Fig. 4), but the results are somewhat different. Fig. 8 plots the values of the feed-forward coefficients (1–6) and feedback coefficients (7–12) for impulse response A at the end of 1000 symbols. The dominant tap coefficients have the same values as that calculated by mmse. Fig. 9 plots the evolution of the feed-forward taps as a function of incoming symbols. We see that (unlike Fig. 6) the values of the feed-forward taps are not stable with time, despite the fact that the channel is time invariant. The fluctuation of the feed-forward coefficients (particularly 6, which is the largest) is

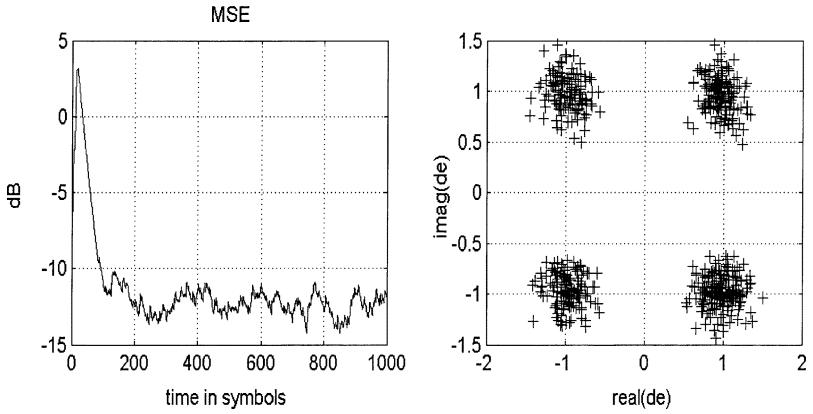

Fig. 7. Symbol mse for impulse response B of Fig. 4 (left). Symbol constellation plot for the estimated symbols, de (right).

responsible for the increased mse and high bit errors, as seen in Fig. 10, which plots the symbol mse and symbol constellations. We note that the mse is now -5 dB, approximately 7 dB higher than the previous case. The symbols in Fig. 10 are more scattered as compared with Fig. 7; there actually are seven symbols in error out of 1000 symbols.

As remarked above, there seems to be little physical differences between impulse responses A and B. The significant differences in the mse and bit errors between the two cases are attributed to the numerical sensitivity of the RLS algorithm (as a result of synchronization error). In the above analysis, the received signals were sampled at one sample per symbol. This is equivalent to sampling the impulse responses in Fig. 4 at the center of the grid. It seems that the impulse response B (and, hence, the resulting ISI) is adequately sampled by this method. For impulse response A, the timing is slightly off for the dominant first and second arrivals (the peaks are slightly off the center), hence the need to update the tap coefficients to adapt to the ISI in the data. Although fractional sampling (e.g., two samples per symbol) is used in real data analysis to minimize the sampling problem, the danger remains that a (small) error will propagate to cause the algorithm to diverge.

The last subject of discussion is the minimum number of feed-forward tap coefficients. Fig. 8 shows that only one or two feed-forward coefficients (5 and 6) are dominant for impulse response A. Fig. 5 shows that only three feed-forward coefficients (4–6) are dominant for impulse response B. The division of feed-forward and feedback coefficients can be traced to the impulse-response functions. For impulse response A (Fig. 4), the first arrival is the largest (minimum phase channel). It covers only one symbol; hence, only one feed-forward coefficient is required (Fig. 8). For impulse response B, the second arrival is the largest. Hence, at least two feed-forward coefficients are required, as shown in Fig. 5.

We see from Figs. 8 and 9 (or Figs. 5 and 6) that the rest of the feed-forward coefficients are small and not really contributing to channel equalization; they could just as well not be included in the first place. Note that the RLS and mmse method do not specify how many feed-forward and feedback coefficients are to be used. Although many feed-forward coefficients are theoretically allowed, the above results suggest that minimum errors are obtained when a minimal number of feed-forward coefficients

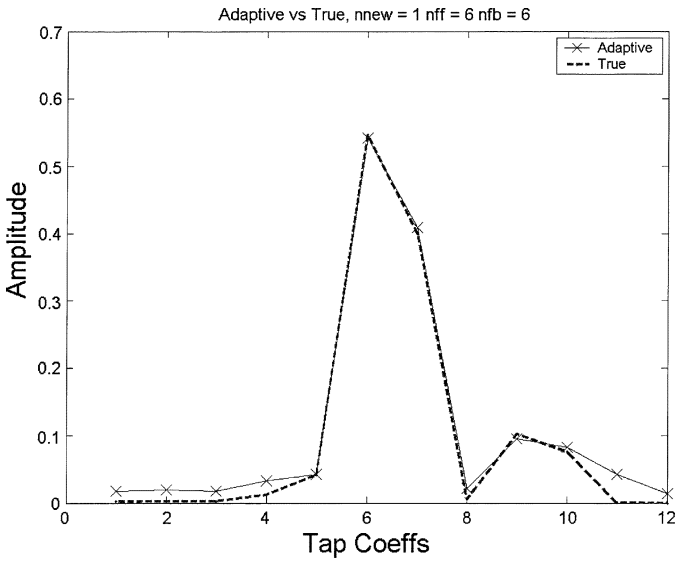

Fig. 8. Comparison of tap coefficients determined by the RLS algorithm ("x" and solid line) and mmse formula (dashed line) for impulse response A of Fig. 4. Feed-forward and feedback are designated by taps 1–6 and 7–12, respectively.

are used. Additional coefficients have the effect of increasing the processor noise. The number of feedback coefficients is constrained by the multipath delay, as remarked above.

IV. Performance Comparison: Simulated Data

The simulated data to be analyzed are the first case discussed in [8]. The data were generated in a range-independent waveguide with a constant sound speed (1500 m/s) profile. It has a water depth of 100 m with a sediment layer of 40 m overlaying a rock bottom, with a sound speed increasing from 1572 to1593 m/s, an attenuation of 0.02 dB/kmHz. The source is placed at a range of 10 km and a depth of 35 m. The vertical line array (VLA) has 15 elements, evenly spaced over a depth from 5 to 75 m. Simulated impulse-response functions showed that multipath arrivals last over $\sim$80 m/s (see [8]). As such, extensive ISIs extending over many ($\sim$40) symbols and, consequently, high BER were found in the raw data.

A pseudorandom binary PSK (BPSK) signal was used for communications; it has a carrier frequency of 750 Hz and a bandwidth of 250 Hz. The BPSK symbols were constructed with three cycles of sine waves at 750 Hz with a phase of either 0 or

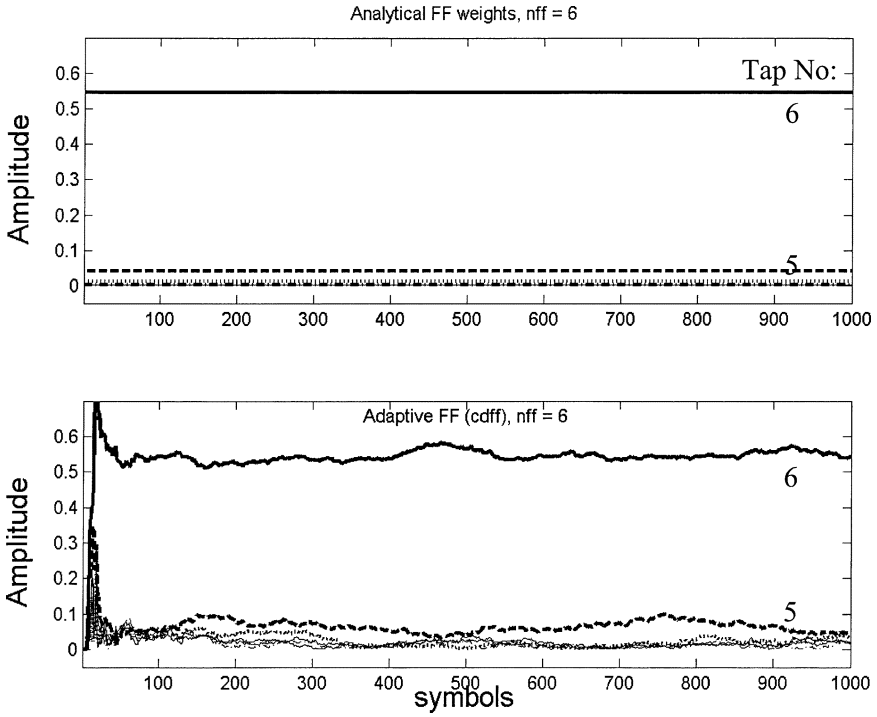

Fig. 9. Evolution of the feedback coefficients as determined by the RLS algorithm (bottom) and mmse solution for impulse response A of Fig. 4 (top).

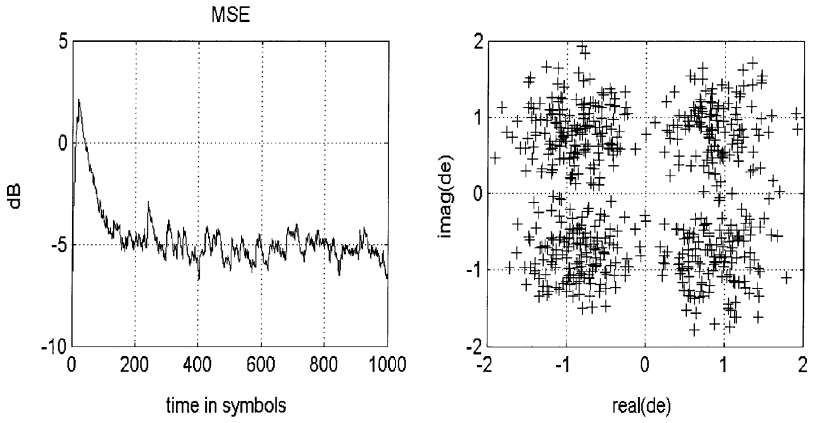

Fig. 10. Symbol mse for impulse response A of Fig. 4 (left) and symbol constellation plot for the estimated symbols, de (right).

180°. The signal is then band-pass filtered to conform to the bandwidth of 250 Hz. The processed data are usually displayed by a symbol constellation plot, which plots the complex values of the symbols. For BPSK signals, the correctly identified symbols should cluster around two locations: $+1$, and -1, on the real axis. A constellation plot with scattered symbols is usually an indication of high BER.

The BPSK signals consisted of a probe signal followed by a gap, then the data package. The data package begins with the training data, followed by the message data. The gap after the probe signal is sufficiently long so that the impulse response of the channel can be estimated from the probe signal. The beginning of the training data (symbol synchronization) is determined by the probe signal. The probe signal uses an m-sequence of 255 symbols.

BER analysis for PPC was discussed in detail in [8]. Here, we will present the results of LE and DFE for comparison with the PPC results. In addition, results of mse and output SNR will also be presented in the performance analysis. Simulated data with different input SNR and different degrees of added random phases were presented in [8] and are used here. We will concentrate on the 10-dB SNR case here and assume that the signal has a random phase with a standard deviation $\sigma = 30°$. (The value is consistent with that measured from at-sea data [8].) For PPC, no bit errors were found for an input signal of 50 dB if the number of receivers exceeds 5. A small-residue BER (1%) was found for input SNR of 10 dB when many (>10) receivers were used. Note that, for the simulated as well as real data analysis below, the signal is band-pass filtered according to the signal bandwidth. We use a bandwidth equaling the data rate. As remarked in [8], BER for PPC can be reduced by increasing the bandwidth or decreasing the data rate.

For DFE and LE, we use a PLL in conjunction with the equalizer, as proposed for underwater acoustic communications. The PLL is used to track the symbol (random) phase change. The PLL is used for the simulated data in conformity with real data

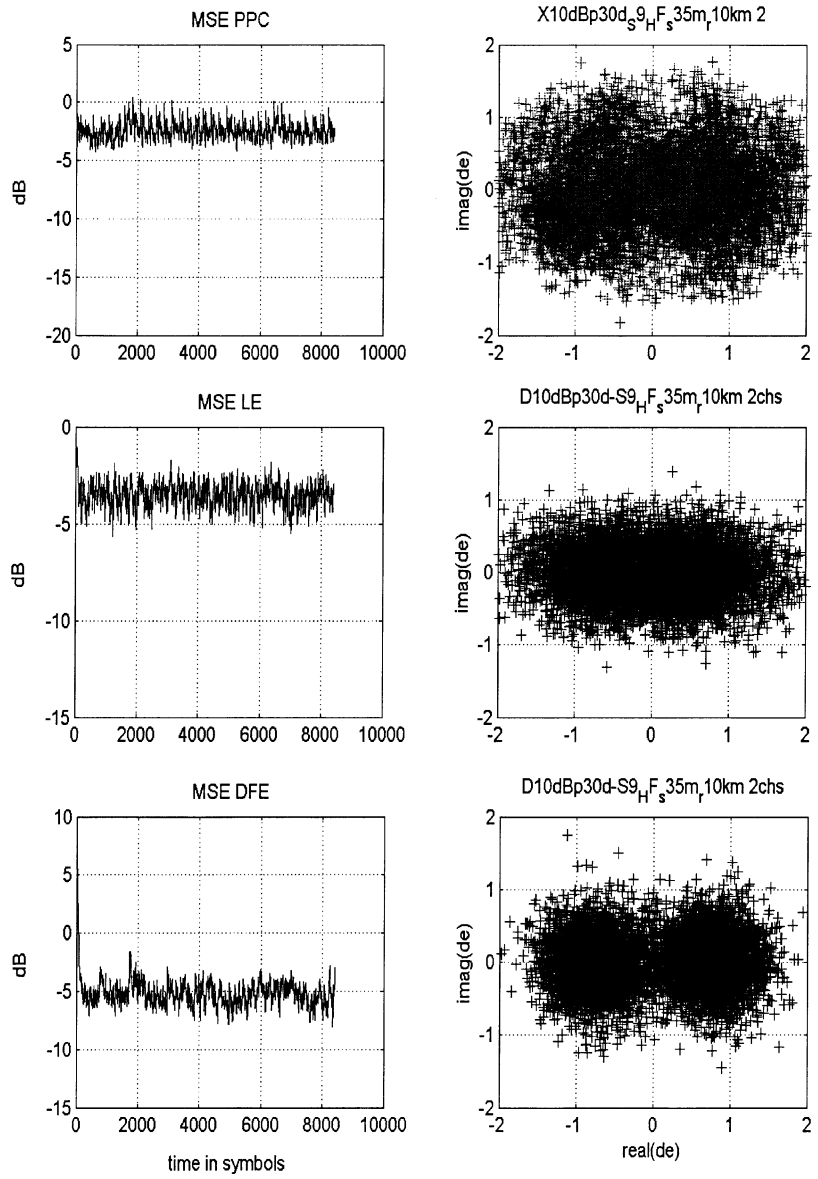

Fig. 11. Analysis of simulated data using the top two receivers. Symbol mse plots are shown on the left and symbol constellation plot for the estimated symbols (de) are shown on the right for the PPC, LE, and DFE processors in descending order.

processing where PLL is required. We also use a sparse equalizer to minimize the number of tap coefficients [14]. The reader is referred to [1] for a review of the detailed algorithm and for further references. For the RLS, we use 0.989 for the forgetting factor. The numbers of feed-forward and feedback coefficients are estimated from the impulse response for each channel with a threshold of -15 dB from the peak; we use 8 and 16, respectively. For PLL, we use 0.001 and 0.0001 for the proportional and integral constants.

Fig. 11 plots the mse (left column) and symbol constellation (right column) results for two channels near the top of the vertical array; results are displayed in descending order for the PPC, LE, and DFE algorithms. The one channel DFE did not converge using the RLS algorithm. We note that PPC has higher mse than LE and that DFE has the least mse. Note that different scales are used in the figures.

Fig. 12 plots the mse and symbol constellation for the PPC, LE, and DFE algorithms for 11 channels in the same format as Fig. 11. We use a maximum of 11 channels for comparison with the data analysis in the next section. As compared with Fig. 11, we see that spatial diversity significantly reduces the mse and symbol cluster size.

In general, we note the following rules are true. The larger the mse, the more the symbols will be scattered in the symbol-constellation plane. Indeed, in Fig. 12 (right column) we see that the symbols are tightly clustered in the DFE case and are widely scattered in the PPC case. (Note that the symbols are symmetrically scattered over the constellation plot for both LE and DFE, but not for PPC, the cause of the asymmetry was given in [8].) Note that more scattering implies a higher chance for symbol misidentification. Consequently, one expects higher BER for PPC than DFE. We will find below that PPC has the most bit errors and DFE has the least bit errors, which is in conformity with the theoretical analysis given above.

Fig. 13 plots the average mse (over data symbols) as a function of number of receivers for the PPC, LE, and DFE cases.

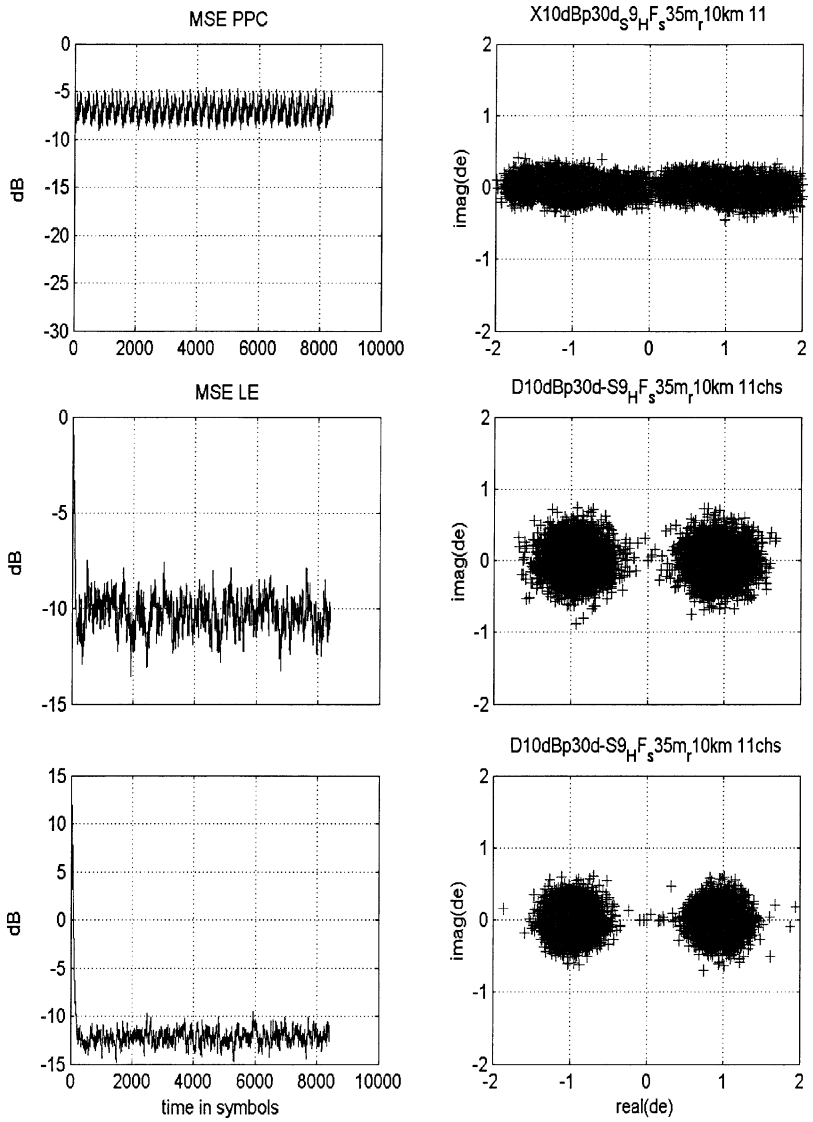

Fig. 12. Analysis of simulated data using 11 receivers. Symbol mse plots (left) and symbol constellation plot for the estimated symbols (de; right) for the PPC, LE, and DFE processors in descending order.

The receiver channels are counted from the top phone on the VLA. We see that PPC has the largest mse, followed by LE, and DFE has the lowest mse, irrespective of the number of receivers used.

Fig. 14 plots the output SNR as a function of the number of receivers for the PPC, LE, and DFE algorithms. Although it is conventionally called output SNR, it actually is the ratio of signal to noise plus ISI. In the case of high SNR, the "noise" will be dominated by the residual ISI in the signal. The output SNR is given by $\mathrm{SNR}_{\mathrm{out}} = (1 - \mathrm{mse})/\mathrm{mse}$ [9].

Fig. 15 plots the BER (of the data symbols) as a function of number of receivers for the PPC, LE, and DFE algorithms. We find that DFE has zero bit errors for $\geq$4 receivers. PPC has a higher BER and approaches the DFE results when the number of receivers increases beyond 6.

We note that LE has a higher BER than PPC when the number of receivers used is less than four. However, for more than four channels, BER for LE quickly decreases to zero and is significantly better than PPC. The former behavior is somewhat surprising. To explain this, we note that the LE results are quite sensitive to the number of tap coefficients used. As remarked above, a LE requires in principle an infinite number of tap coefficients. For dependence on the number of tap coefficients, we refer the reader to [15], where the performance of two multichannel LEs were previously studied in great detail. It is noted there that mse and BER vary significantly with respect to the number of diversity channels and the length of the equalizer coefficients. For the same mse, or BER, fewer tap coefficients are needed when more diversity channels are used. In this study, we used a fixed number of tap coefficients for all diversity channels. Apparently, the number of taps coefficients (multipath delay plus five symbol lengths) used was not enough for $<$4 channels. We did not attempt to optimize the LE, since our interest lies mainly in the comparison between PPC and DFE; the LE results were included for reference.

We note that the algorithm performance will depend on the SNR of the received signal and the signal-random phase. In the above analysis, we assumed that the signal has an input SNR of 10 dB and a random phase with a standard deviation $\sigma = 30^{\circ}$. To study how the various algorithms perform with respect to

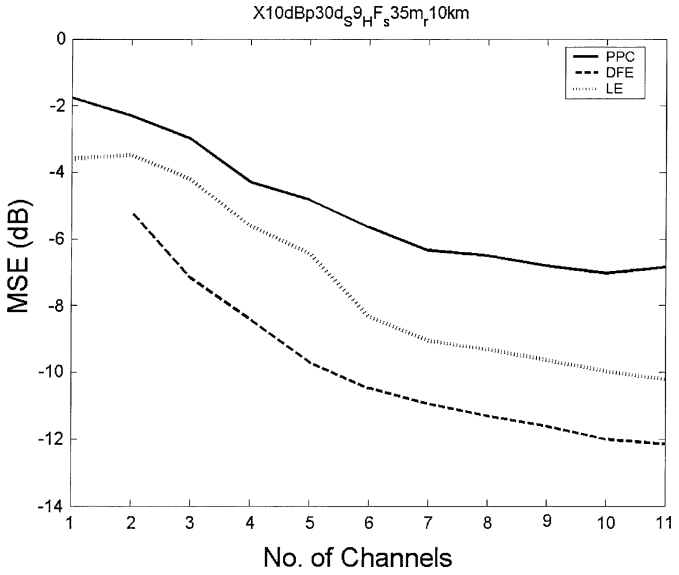

Fig. 13. The mse as a function of the number of receivers for PPC (solid line), LE (dotted line), and DFE (dashed line) for the simulated data.

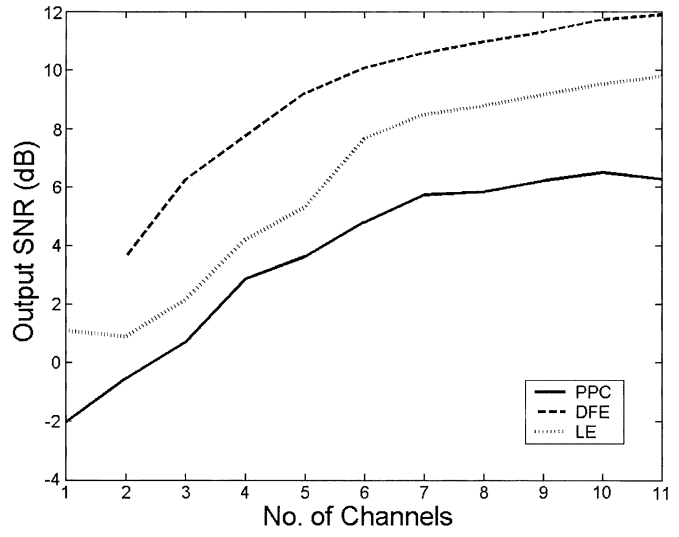

Fig. 14. Output SNR as a function of the number of receivers for PPC (solid line), LE (dotted line), and DFE (dashed line) for the simulated data.

different signal-random phases, we assume high-input SNR (50 dB) so that noise is not an issue. Fig. 16 plots mse as a function of the number of receivers for $\sigma = 0°$, $10°$, $20°$, and $30°$ using DFE [see Fig. 16(a)] and PPC [see Fig. 16(b)]. We note that DFE is much more sensitive to the signal-random phase than PPC. Significant improvement in mse is obtained for DFE as σ decreases. PPC, on the other hand, is rather insensitive to the signal-random phase, but it yields a significantly higher mse than DFE. For DFE with a single receiver, one obtains a zero and near-zero BER using only for $\sigma = 0°$ and $10°$, respectively. BER is zero when two or more receivers are used. For $\sigma = 20°$ and $30°$, zero BER requires two, three, or more receivers. We did not explicitly show the BER results, but the result can be obtained from mse using a rule of thumb: BER for DFE is generally zero when mse goes below -8 to -10 dB. We observe that BER for PPC remains relatively high until many (>5) receivers are used.

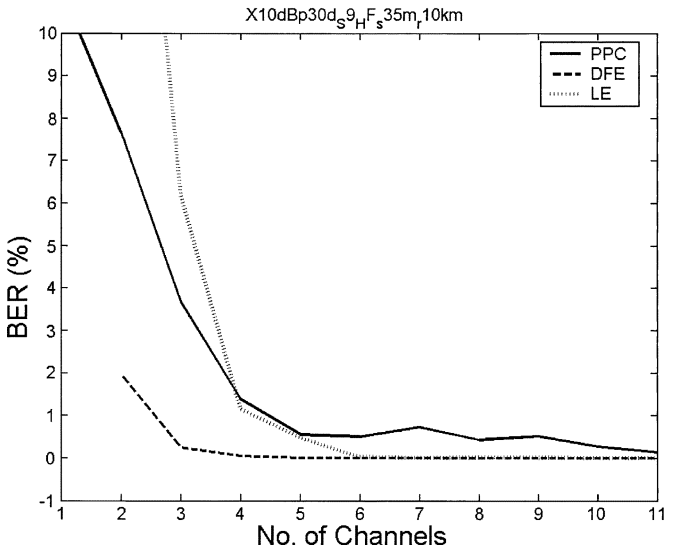

Fig. 15. BER as a function of the number of receivers for PPC (solid line), LE (dotted line), and DFE (dashed line) for the simulated data.

To study how the various algorithms perform with respect to different SNR, we assume that $\sigma = 10°$ and plot mse as a function of the number of receivers in Fig. 17 for input $\mathrm{SNR} = 10$, 20, and 50 dB. Again, we see that for DFE, mse improves as input SNR increases [see Fig. 17(a)]. We find that, for a single receiver, BER is 40%, 0.16%, and 0.025% for $\mathrm{SNR} = 10$, 20, and 50 dB, respectively. BER is zero for all cases when two or more receivers are used. Fig. 17(b) plots the mse for PPC. We find that for PPC, mse remains at approximately the same level despite increasing SNR. The mse for PPC is significantly higher than mse for DFE. BER is zero when five or more receivers are used.

V. Performance Comparison: At-Sea Data

We use the same at-sea data analyzed in [8] and apply the three different processors to analyze the performance difference. Data were collected off the coast of New England by the NATO SACLANTCEN in June 2001 [16] during the ASCOT 01 experiment. Sixteen channels of the VLA were used, covering a depth of 30–90 m. Of the 16 channels, we selected 11 channels that are close to being uniformly spaced. The VLA was deployed in water of 99.2-m depth. The source was deployed 4 m above the bottom; the bottom depth is 103 m and the source–receiver range is approximately 10 km. BPSK signals of a bandwidth of 500 Hz were transmitted with a carrier frequency of 3550 Hz. The reader is referred to [8] for discussions of the signal characteristics and to [16] for details of the oceanographic data collected during the experiment.

Fig. 18 (right) plots an impulse-response function collected on one of the receivers for comparison with the impulse-response function for the simulated data (left). The impulse-response function was deduced from the probe signal for the data processed below. We note that the two impulse-response functions have approximately the same multipath spread (<25 symbols) and the same number of paths, but with a different delay structure. For the ASCOT 01 data, we use ten feed-forward and 25 feedback coefficients. The parameters for DFE and PLL are the same as mentioned in Section IV.

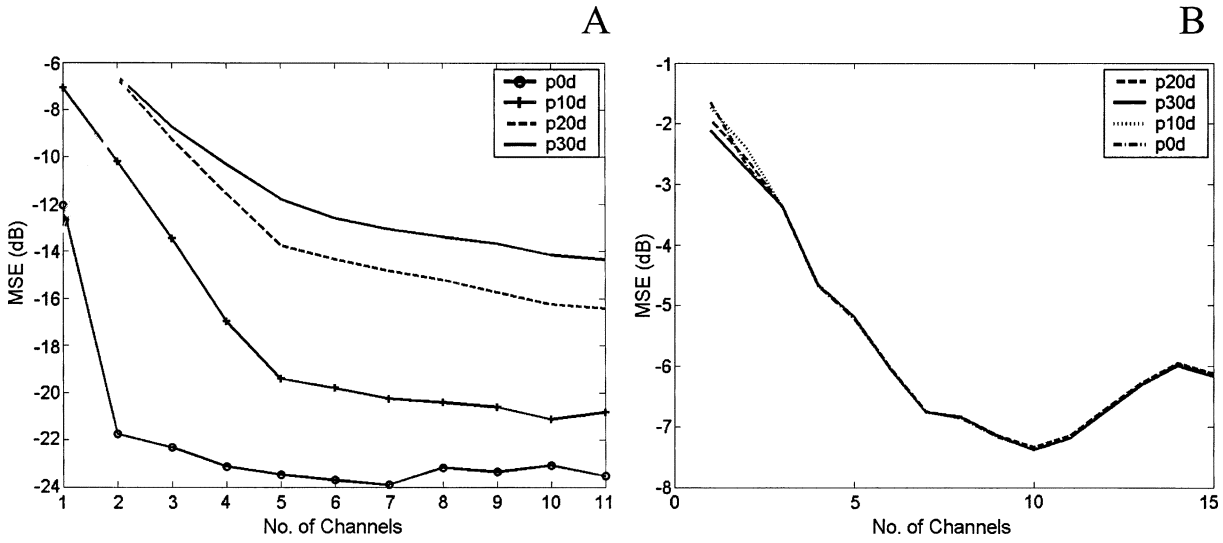

Fig. 16. The mse as a function of the number of receivers: sensitivity to the random-symbol phase with $\sigma = 0°, 10°, 20°$, and $30°$. (a) DFE and (b) PPC, respectively.

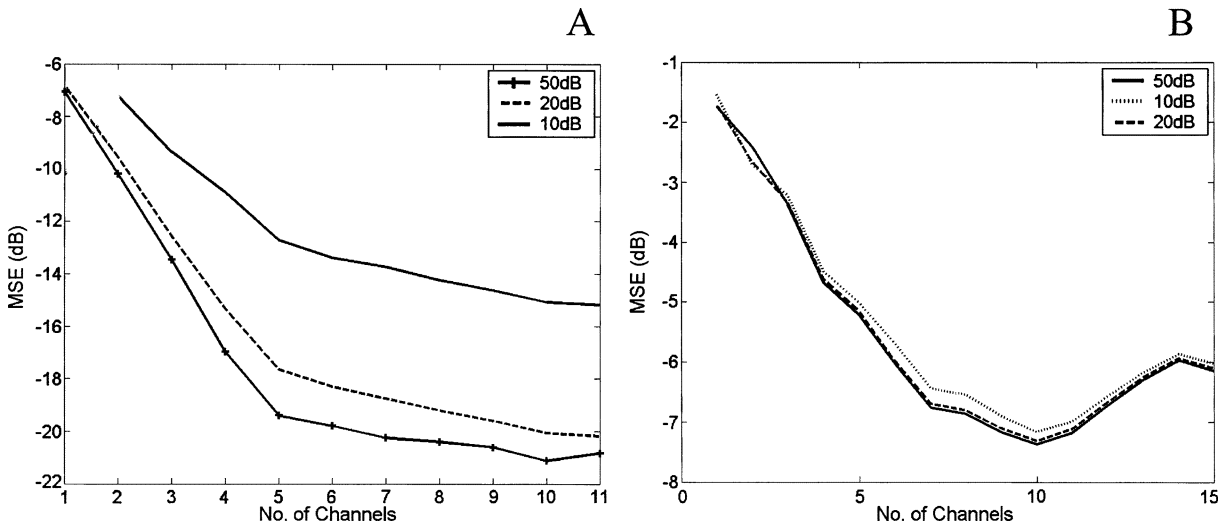

Fig. 17. The mse as a function of the number of receivers: dependence on the SNR for (a) DFE and (b) PPC.

Figs. 19–21 plot the mse, output SNR, and BER as a function of number of the receivers, counting from the bottom of the vertical line array. Comparing Fig. 19 with Fig. 17(a) for DFE and noting that the input SNR in the data is ∼20 dB, we find that the measured mse for the data is a few (2–4) dB higher than the simulated result. One notes that the general behavior agrees with the simulated data well. There are differences in the details, since the acoustic environments are different for the two cases. This suggests that the performance between PPC and DFE could be modeled. Note that the difference between PPC and DFE lies in the residual ISI (18), which is caused by nonzero sidelobes of the Q function when the number of receivers is small. The Q function can be calculated for a given acoustic environment and receiver positions. The resulting ISI (hence, the mse, BER, etc.) can therefore be modeled for both simulated and real data.

A. Processor Update versus Channel Update

Next, we turn to a different subject. The comparative analysis of the ASCOT data using PPC versus DFE reveals a somewhat surprising result that deserves investigation. The ASCOT data showed that the acoustic channel was very coherent over the packet length of 17 s, i.e., the impulse-response function changed little with time [8, Fig. 15]. Using PPC, the 17-s data were decoded using one probe signal [8], suggesting that the channel was nearly time invariant. The only exception is that the symbols had a mean phase that increased with time at a rate of 0.56 rad/s, which was measured and removed from the data. For DFE and LE, the symbol mean phase was removed using PLL in conjunction with the equalizer.

If the channel is time invariant, the values of the feed-forward and feedback coefficients should stay constant with time (after training). In other words, the channel should require very little updating. One finds, however, when PLL and DFE were applied to the ASCOT data, the RLS algorithm was updated more than 98% of the time, i.e., the tap coefficients were updated for >98% of the symbols (when mse exceeds −7 dB). We plot the time evolution of samples of feed-forward and feedback coefficients in Fig. 22, which shows that the values are constantly changing

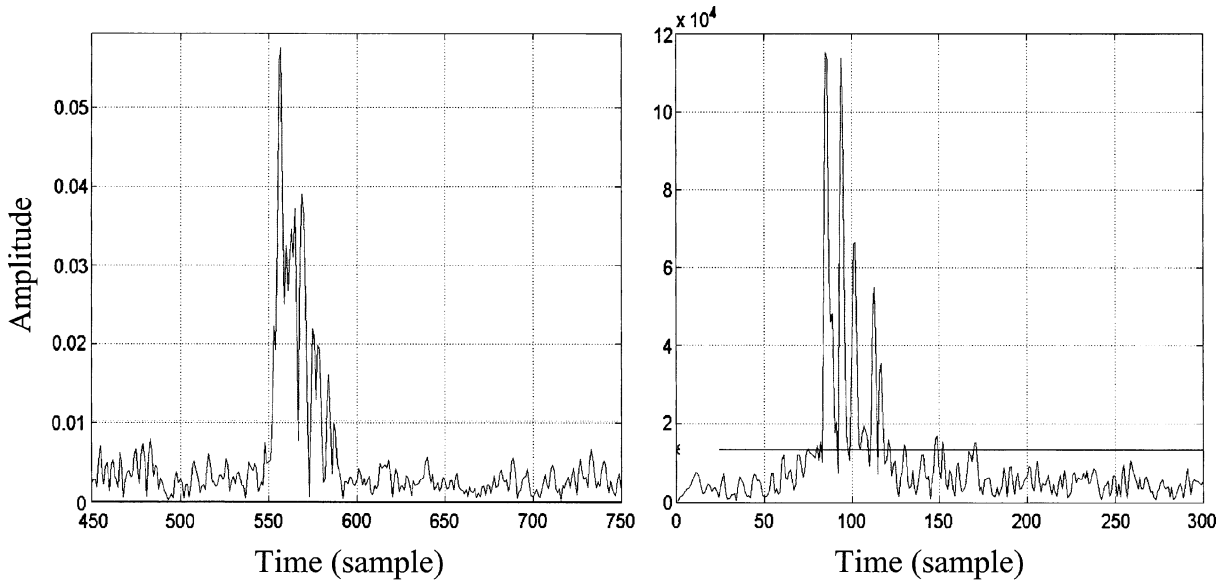

Fig. 18. Comparison of impulse-response functions for (left) simulated data and (right) ASCOT data. Two samples per symbol.

with time, confirming the need for a rapid update. Some explanations are required.

Past experiences (by many people) have also shown that the RLS algorithm encountered $>98\%$ update in most of the data packets analyzed. The observed high (data) update rate has suggested (to many) that the underwater acoustic communication channel at the communication frequencies encounters rapid changes at the rate of a few symbols to tens of symbols. This implication seemed a little bit odd, as one found it difficult, albeit not impossible, to find a physical reason for the rapid change at carrier frequencies <5 kHz [17]. However, no counter argument was found to dispute the data-analysis results. The implication of a rapidly changing channel has prompted many to suggest the need for a better channel-tracking method.

Motivated by the above discussions, several experiments have been conducted to measure the temporal coherence of an underwater acoustic channel. The measurements were carried out using a fixed source and receivers so that platform motion was not an issue. Results from two experiments [18]–[20] have shown that the channel has a coherence time (for coherence, >0.5) greater than $5. \times 10^4 f^{-1}$ s at a range of 10 km, for $f < 5$ kHz. The conclusion is that in general the channel is coherent over the length of the signal packet. In other words, the channel could not be changing at a rapid rate, as indicated by the DFE update results.

To resolve the issue, one needs a simultaneous measurement of the temporal coherence and an analysis of the data using DFE. This was done using BPSK signals with repeated m-sequences. The evolution of the impulse-response function with time is measured using the m-sequence and the data is processed using DFE. The impulse-response functions for the ASCOT data were shown in [8, Fig. 15] and the DFE results applied to the same data were shown above.

Now, we will try to explain the results. We suspect that the rapid update encountered by DFE is due to the nonlinear interactions between the DFE and PLL. The ASCOT data have clearly demonstrated [8] that the channel impulse-response function is nearly time invariant (or is slowly changing with time) within a packet. However, the rapid phase rate of the symbols (0.56 rad/s) implies that DFE will not work without first removing the phase change. The RLS algorithm should, in principle, adapt to the phase change, but, as shown above, it requires 20–30 symbols to converge, during which time the symbol phase has changed substantially. It was determined that RLS could not remove the rapid phase and that a combined use of PLL with DFE was required.

What should work in theory (for the above case) is that PLL should remove the rapid phase change and that DFE should be time invariant. Note that, in RF communications, PLL can be used separately to recover the carrier frequency (including shift), but in underwater acoustic communications, PLL needs to be used jointly with DFE on a symbol-by-symbol basis [1]. In that case, one observes that both PLL and DFE are competing to compensate for the rapid symbol-phase variation. Consequently, the nonlinear interaction between PLL and DFE causes DFE to be updated $>98\%$ of time. This is what happened in the above data analysis and can be independently verified using simulated data (not shown here).

The conclusion from this study is that the high update rate observed in data analysis (channel equalizer) is likely an artifact of the processor (the forced marriage between the PLL and DFE operators) and does not imply an equally fast change in the ocean acoustic channel.

For data collected from a moving platform, one finds that the coherence time can be substantially reduced by the platform motion when Doppler is not correctly estimated [20]. In that case, the $>98\%$ update is almost a must with the consequence of a larger mse than when the Doppler is correctly estimated. This shows another aspect of the problem concerning DFE, namely the need for accurate Doppler estimation [21].

VI. Summary and Discussion

In this paper, we presented the PPC, LE, and DFE using a common framework. Both PPC and LE use a linear transversal filter. In the former case, the filter coefficients are matched to

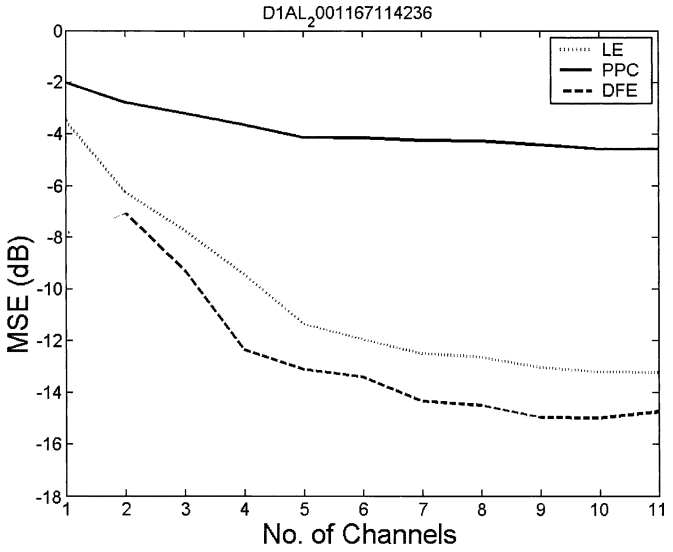

Fig. 19. The mse as a function of the number of receivers for (solid line) PPC, (dotted line) LE, and (dashed line) DFE for the ASCOT data.

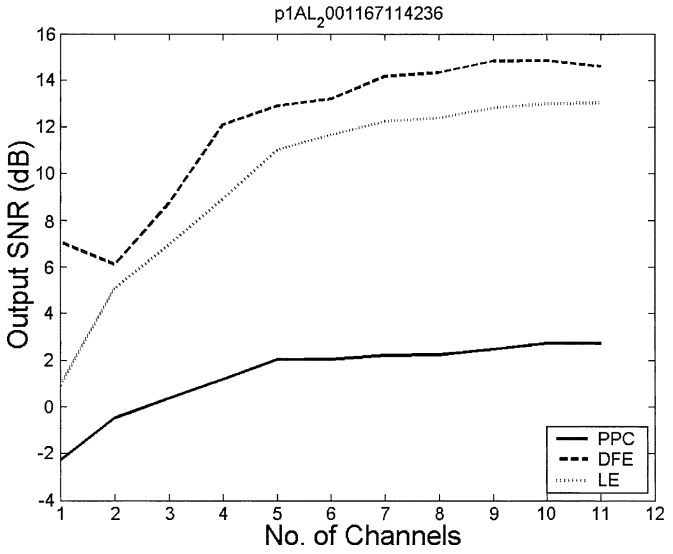

Fig. 20. Output SNR as a function of the number of receivers for (solid line) PPC, (dotted line) LE, and (dashed line) DFE for the ASCOT data.

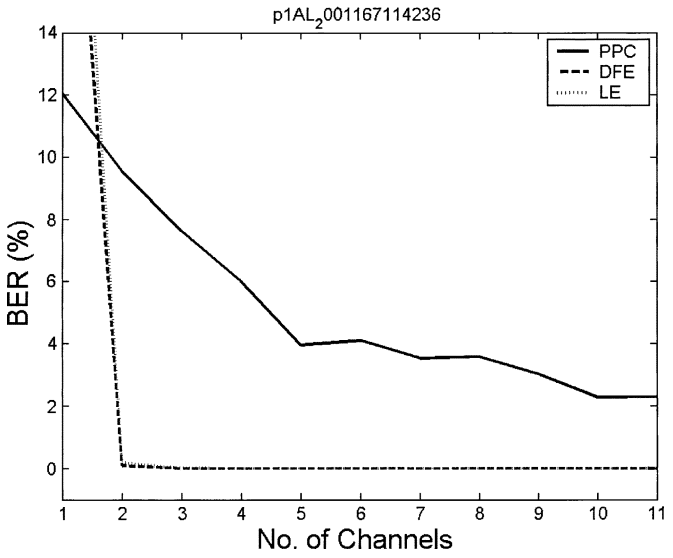

Fig. 21. BER as a function of the number of receivers for (solid line) PPC, (dotted line) LE, and (dashed line) DFE for the ASCOT data.

the time-reversed impulse-response function for each receiver channel. In the latter case, the filter coefficients are determined by the mmse criterion (see Figs. 1 and 3). Although the PPC solution does not yield the minimum mse, by summing over many receivers over a large aperture vertical array, ISI is minimized by the physics of waveguide propagation. The wave equation dictates that the Green's functions from a source to receivers convolved with their time-reversed conjugates, summed over a large aperture vertical array of receivers (the Q function) behaves like a delta function in space and time.

We showed that, for a small number of receivers, PPC could not remove all the ISI. It requires an additional "feedback" loop (18). We showed in [8] that the BER can be reduced to a minimum when the peak sidelobe level of the Q function is below 10% of the main lobe level. In that case, we find that the error correction due to the feedback loop is minimal and that PPC performs approximately the same as the multichannel DFE. The advantage of DFE is its ability to reduce the mse and BER compared with PPC and LE when the number of receivers is small. It yields a higher output SNR. In general, DFE outperforms PPC and LE in terms of mse, BER, and output SNR.

The mmse solution was used for DFE to compare with the PPC and LE results. We note that the mmse criterion does not specify how many feed-forward and feedback coefficients are to be used. Without the noise, one can use as many as desired to remove the ISI. With noise, too many taps effectively increase the noise level; hence, a minimal number of taps should be used. We showed that the number of feedback coefficients should equal the number of multipaths measured in terms of symbols minus one (counting from the main arrival). The number of feed-forward coefficients should equal the multipath arrivals in symbols before the main arrival. This rule of thumb was illustrated using simulated data.

The mmse solution requires the inversion of a large matrix and is not practical when the multipath is long and the channel is time varying. An RLS algorithm is commonly used for a time-varying channel and is widely used in practice due to its fast convergence rate. We showed that the RLS algorithm yields the same numerical answer as the mmse solution for a time-invariant channel. RLS was then used to analyze simulated data in a realistic ocean as well as at-sea data. The data (performance) analysis is concerned with the determination of mse, output SNR, and BER as a function of number of receivers using the various (PPC, LE, and DFE) methods.

As expected, the simulated data showed that DFE outperforms PPC in mse, output SNR, and BER when the numbers of receivers are small. The difference in performance is due to the residual ISI. The LE performance is more sensitive to the number of taps used. An LE is included for comparison purpose. We note that the BER approaches zero for all processors when the number of receivers increases, because spatial diversity reduces ISI and symbol-phase variance, as discussed in [8].

Thus, in theory DFE works better than PPC, particularly when only a small number of receivers are used. However,

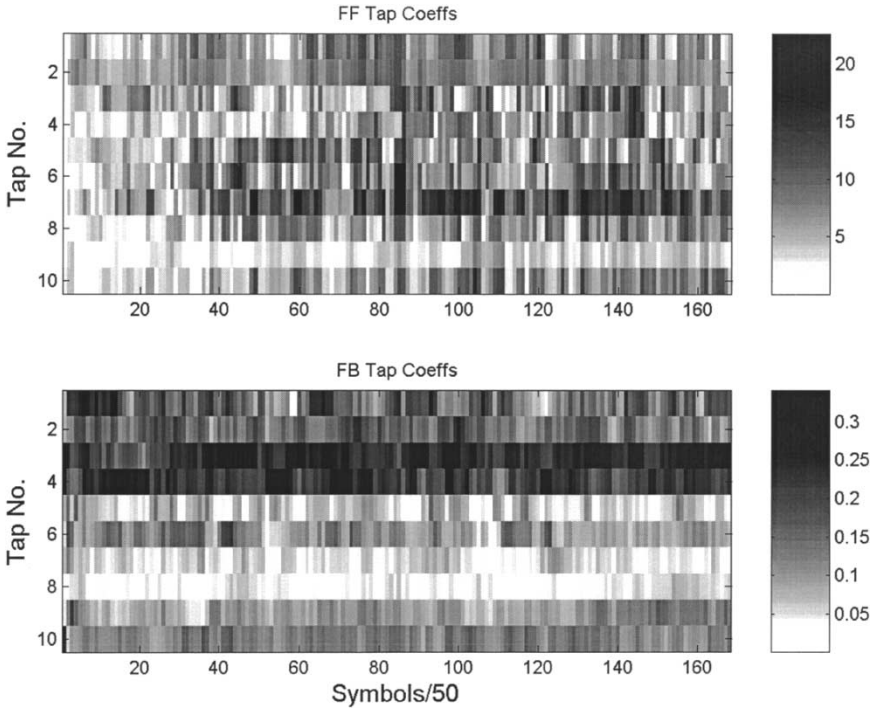

Fig. 22. Time evolution of feed-forward tap coefficients, single channel (top) and first ten feedback tap coefficients (bottom) for the ASCOT data using a four-channel DFE that yields zero bit error.

DFE has its own problems, such as numerical sensitivities to the number of taps used, the estimation of the channel impulse function and Doppler shift, etc. The DFE algorithm has been shown to work with real data, but it sometimes does not converge (due to the well-known error-propagation problem) and requires certain parameter adjustments. The error-propagation problem has limited the use of unsupervised adaptation of the DFE in real communication systems. The DFE works well only when data possess high temporal coherence [12].

We found that the performance analysis for the at-sea data showed the same trend and values in terms of the difference (in mse, output SNR) between PPC and DFE as the values measured from the simulated data. This is not a surprise, since the difference in performance between PPC and DFE is due to the residual ISI (18) caused by the sidelobes of the Q function and the measure and simulated Q functions are very close to each other. Consequently, the difference in performance can be modeled and predicted. While the simulated and real data have a different carrier frequency, they have a similar impulse response in the baseband. The above analysis showed that the performance difference is determined by the Q function in the baseband. Hence, it is not a surprise to find similar result between simulated and real data. Although only one example was given for each case, the analysis based on the Q function implies that the results can be generalized to other cases.

Finally, we note that while the performance of DFE has been analyzed extensively for a radio-communication channel, modeling the DFE performance directly for an ocean acoustic channel has been difficult. (No theoretical or numerical analysis has been presented to this date.) In [8], we provided a modeling capability for PPC for an underwater acoustic channel. In this paper, we modeled the performance difference between PPC and DFE. Performance prediction for DFE can be obtained by combining the two works together.

ACKNOWLEDGMENT

The author would like to thank SACLANTCEN for conducting the ACOMMS tests during the ASCOT 01 experiment, W.-B. Yang for helpful discussions, and K. Bell for assistance during the early phase of the work.

REFERENCES

[1] M. Stojanovic, "Recent advances in high-speed underwater acoustic communications," *IEEE J. Oceanic Eng.*, vol. 21, pp. 125–136, Apr. 1996.

[2] G. F. Edelmann, W. S. Hodgkiss, S. Kim, W. A. Kuperman, H. C. Song, and T. Akal, "Underwater acoustic communication using time reversal," in *Proc. OCEANS'01*, 2001, pp. 2231–2235.

[3] T. C. Yang, "Method and System for Sensing With an Active Acoustic Array," U.S. Patent 5 535 176, July 1996.

[4] D. Rouseff, D. R. Jackson, W. L. J. Fox, C. D. Jones, J. A. Ritcey, and D. R. Dowling, "Underwater acoustic communication by passive-phase conjugation: Theory and experimental results," *J. Oceanic Eng.*, vol. 26, pp. 821–831, Oct. 2001.

[5] A. Silva, S. Jesus, J. Gomes, and V. Barroso, "Underwater acoustic communication using a "virtual" electronic time-reversal mirror approach," in *Proc. 5th Eur. Conf. Underwater Acoustics*, M. E. Zakharia, Ed., Lyon, France, July 2000, pp. 531–536.

[6] W. A. Kuperman, W. S. Hodgkiss, H. C. Song, T. Akal, C. Ferla, and D. R. Jackson, "Phase conjugation in the ocean: Experimental demonstration of an acoustic time-reversal mirror," *J. Acoust. Soc. Amer.*, vol. 103, pp. 25–40, 1998.

[7] D. R. Dowling, "Acoustic pulse-compression using passive phase-conjugation processing," *J. Acoust. Soc. Amer.*, vol. 95, pp. 1450–1458, 1994.

[8] T. C. Yang, "Temporal resolution of time-reversal and passive-phase conjugation for underwater acoustic communications," *IEEE J. Oceanic Eng.*, vol. 28, pp. 229–245, 2003.

[9] J. G. Proakis, *Digital Communications*, 3rd ed. New York: McGraw-Hill, 1995, ch. 10.

[10] B. Widrow and S. D. Stearns, *Adaptive Signal Processing*. Englewood Cliffs, NJ: Prentice-Hall, 1985, ch. 8.
[11] S. Haykin, *Adaptive Filter Theory*, 3rd ed. Englewood Cliffs, NJ: Prentice-Hall, 1996, ch. 13.
[12] T. C. Yang and A. Al-Kurd, "Performance limitations of joint adaptive channel equalizer and phase locking loop in random oceans: Initial test with data," in *Proc. OCEANS'00*, vol. 2, 2000, pp. 803–808.
[13] W.-B. Yang, private communication, 2003.
[14] M. Johnson and L. Freitag, *The Acoustic Communications Toolbox*. Woods Hole, MA: Acoustic Systems Group, Woods Hole Oceanographic Institution, 1996.
[15] Q. Wen and J. A. Ritcey, "Spatial diversity equalization applied to underwater communications," *J. Oceanic Eng.*, vol. 19, pp. 227–241, Oct. 1994.
[16] J. Sellschopp, P. Nielsen, and M. Siderius, "Combination of acoustics with high-resolution oceanography," in *Proc. NATO SACLANTCEN Conf. Impact of Littoral Environmental Variability on Acoustic Prediction*, Lerici, Italy, Sept. 2002.
[17] *Proc. Office Naval Research ACOMMS Workshop*, Victoria, BC, Canada, Sept. 1999.
[18] T. C. Yang and M. Siderius, "Temporal coherence and fluctuation of acoustic signals in shallow water," in *Proc. 5th Eur. Conf. Underwater Acoustics*, Lyon, France, July 11–14, 2000, pp. 63–68.
[19] T. C. Yang, K. Yoo, and M. Siderius, "Internal waves and its effect on signal propagation in the Adventure Bank," in *Proc. 8th Int. Congr. Sound Vibration*, Hong Kong, July 2–6, 2001, pp. 3001–3008.
[20] T. C. Yang, "Temporal fluctuations of broadband channel impulse functions and underwater acoustic communications at 2–5 kHz," in *Proc. IEEE/MTS OCEANS'02*, vol. 4, Biloxi, MS, Oct. 2002, pp. 2395–2400.
[21] ——, "Underwater Telemetry Method Using Doppler Compensation," U.S. Patent 6 512 720, Jan. 2003.

T. C. Yang has worked on a wide spectrum of acoustics problems in the Arctic from 1979 to 1993. He was responsible for the array wet-end design for an ice-mounted surveillance system. Since 1993, he has worked on the geoacoustic inversion of ocean-bottom properties, sonar array processing, and underwater acoustic communications. He has pioneered matched-mode processing for a vertical line array and recently developed matched-beam processing for horizontal line-array systems. He has published many new findings on ice-edge noise hot spots, underice reflectivity, low-frequency sound-transmission loss, scattering and reverberation, ambient noise coherence and directionality, ice-floe vibrations, and geophone array response and has numerous patents.

Dr. Yang has received a Research Publication Award and is a Fellow of the Acoustical Society of America.